Bamboo-Based Biofoam Adsorbents for the Adsorption of Cationic Pollutants in Wastewater: Methylene Blue and Cu(II)

Chongpeng Qiu, Xuelun Zhang, You Zhang, Qi Tang, Zihui Yuan, Cornelis F. De Hoop, Jiwen Cao, Shilin Hao, Ting Liang, Feng Li,* and Xingyan Huang*

Read Online

ACCESS | Metrics & More | Article Recommendations

ABSTRACT: Human health is being threatened by cationic pollutants in wastewater, for example, methylene blue (MB) and Cu(II). Our research team successfully fabricated biofoam adsorbents from recycled bamboo waste that removed cationic pollutants via introducing bamboo fiber sources, *i.e.*, bamboo fiber, bamboo α-cellulose fiber, and bamboo nanocellulose fiber, into a polyurethane (PU) foam matrix. The biofoam adsorbent with 1 g of nanocellulose (PUN$_1$) presented high removal efficiencies for MB (95.52%) and Cu(II) (100%) in low cationic pollutant concentration aqueous solutions. The biofoam adsorbent with 1 g of bamboo fiber (PUB$_1$) also displayed excellent removal efficiency for MB (98.61%) at pH 11. Meanwhile, 100% removal of Cu(II) was obtained by PUB$_1$ at pH 7 (initial content = 15 mg/L). Furthermore, the PUN$_1$ sample had excellent reusability, evidenced by 61.25% removal of MB after five adsorption−desorption cycles, suggesting that PUN$_1$ is a promising renewable adsorbent for cationic pollutants. In addition, PUB$_1$ is a low-cost adsorbent with good adsorption efficiencies for MB in weak alkaline solutions and Cu(II) in neutral aqueous solutions.
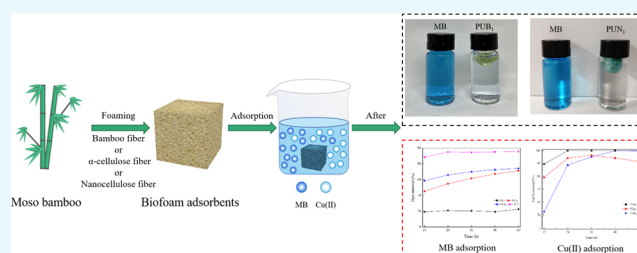
1. INTRODUCTION

Cationic pollutants in wastewater, including cationic dyes and heavy metal ions, such as methylene blue (MB) and Cu(II), have been the major environmental issue,[1] threatening human health.[2] As an important dye used for printing calico, dyeing leather, and cotton, MB has a variety of harmful effects, such as irritation to the gastrointestinal tract, skin burn, and eye burn.[3] Cu(II), a toxic heavy metal ion, is considered nonbiodegradable. Many diseases, such as cancer, kidney damage, development retardation, autoimmunity, and even death, are related to Cu(II).[4] Therefore, the treatment of cationic pollutants in wastewater is very urgent.[5]

Commonly used methods to treat cationic pollutants are ion exchange, membrane filtration, precipitation, and adsorption.[6] Adsorption is the most effective and low-cost way to remove cationics because of its high adsorption efficiency and recyclability.[7] Oxide minerals, charcoal, and clay can be used as adsorbents to purify aqueous solutions of cationic pollutants.[8] However, they are powders, suffering from the disadvantages of poor recyclability, secondary pollution, and a high-cost operation process due to their suspended dispersive property in water.[9] Moreover, activated carbon and synthetic polymers could be used for cationic pollutant adsorption as well,[10,11] while their poor environmental compatibility, non-renewability, and low biodegradability have been obstacles for practical applications.[12] Therefore, it is necessary to produce a

porous adsorbent with a three-dimensional structure, bio-degradability, and multiple porosity.

Bamboo is a cheap, renewable, and abundant lignocellulosic-based biomass resource in China.[13] It has various applications, such as food sources, building materials, and other types of versatile raw biomass.[14] Bamboo plays an important role in the local economy in the Southwest of China. However, a large quantity of bamboo wastes is produced with the development of the bamboo processing industry.[15] The bamboo fiber contains a large amount of lignocellulose. It can be converted into lignocellulose-based high-value products. However, it is difficult to be used for any specific applications due to its small size shape and dry structure.[16] Therefore, it is essential to take further exploration of bamboo waste in potential high-value applications.

The lignocellulose-based adsorbents are well known in wastewater treatment,[17] for example, biochar, cellulose, and lignin-derived adsorbents.[18,19] These bamboo-derived adsorbents have highly efficient environmental, and economic
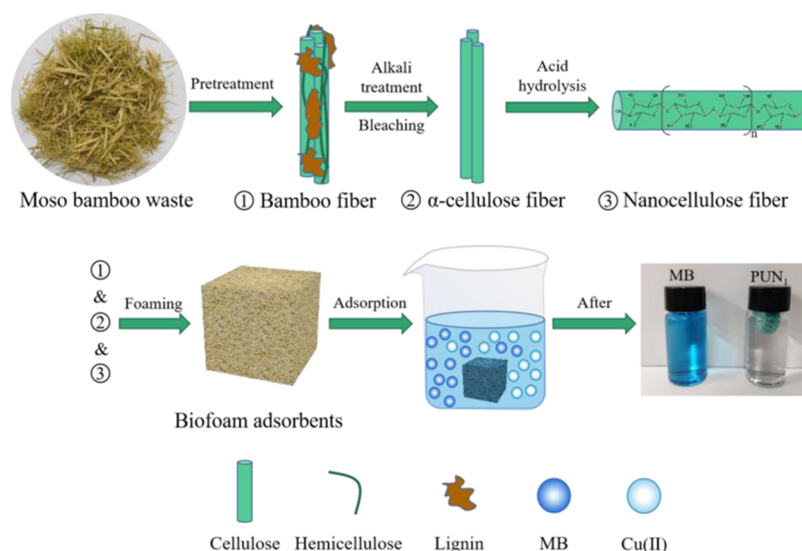
Figure 1. Preparation process of biofoam adsorbents with bamboo fiber sources.

values.[20] However, it is difficult to separate the bamboo-derived adsorbents from wastewater due to their small size and shape.[21] One of the practical approaches to solve this issue is to embed bamboo fiber sources into a polymer matrix. The polymer matrix could allow the adsorbents interact freely with cationic pollutants, and it can be separated from water easily.[22] The polymer matrix should feature good porosity and have a stable structure in water.

Polyurethane (PU) foam has played a critical role in daily life by virtue of its tunable porous structure, excellent strength, and lightweight.[23,24] Therefore, it is possible to apply PU foam as the adsorbent matrix. In fact, it has been used as a matrix for immobilizing various adsorbents, nanocellulose, active carbon, and clays.[25,26] The adsorption capacity of foam-based adsorbents highly depends on the adsorbent, rather than a PU foam matrix.[27] Unfortunately, there is a shortage of efforts to produce bamboo-based biofoam adsorbents for removing heavy metals and dyes from aqueous solutions.

In this work, bamboo fiber sources (bamboo fiber, α-cellulose fiber, nanofiber) were embedded into the PU foam matrix to prepare biofoam adsorbents. The preparation process of biofoam adsorbents is illustrated in Figure 1. The main objective of this study was to prepare high-efficiency biofoam adsorbents to remove MB and Cu(II) from wastewater. The novelty of this work is to figure out the possibility to produce low-cost biofoam adsorbents from bamboo fiber sources with good capacities to remove cationic pollutants from wastewater. Furthermore, the adsorption mechanism of cationic pollutants by biofoam adsorbents was interpreted in this work.

2. RESULTS AND DISCUSSION

2.1. FTIR of Bamboo Fiber Sources.
Fourier transform infrared (FTIR) spectra of bamboo fiber sources are shown in Figure 2. The broad band at around 3690 cm^{-1} corresponded to the $-$OH stretching vibration.[28-30] After alkali and bleach treatments, the peaks of acetyl and uronic ester groups in hemicellulose at 1730 cm^{-1} and the aromatic ring vibration in lignin at 1450 cm^{-1} were absent from α-cellulose and nanocellulose.[31,32] The peak at 1300 cm^{-1} was assigned to O$-$H plane bending in cellulose.[33] The enhancement of hydroxyl groups of α-cellulose and nanocellulose at 3690 cm^{-1}
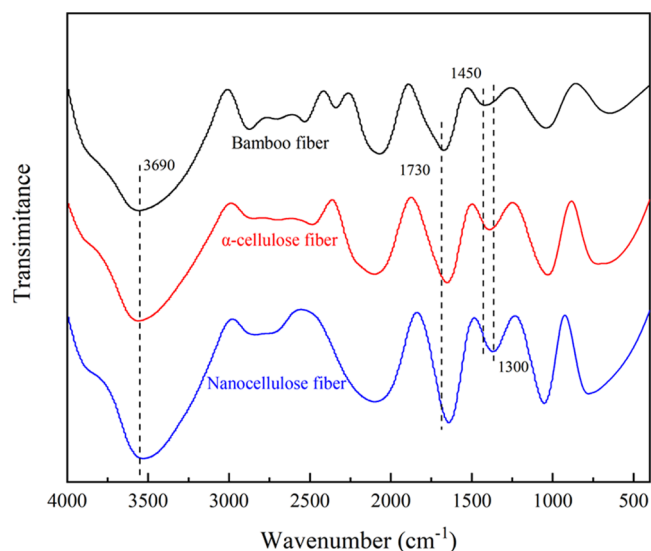

Figure 2. FTIR spectra of bamboo fiber sources.

was ascribed to the removal of noncelluloses.[30] Consequently, FTIR spectra of bamboo fiber sources evidenced that the purification process was successfully conducted by removing noncelluloses.

2.2. Foaming Process.
Table 1 illustrates the foaming process. The start time of reaction between polyols and

Table 1. Gel Time and Rise Time of Biofoam Absorbents

absorbents ID	gel time (s)	rise time (s)
PU$_0$	9.42 ± 0.18	43.53 ± 4.11
PUB$_{0.2}$	8.31 ± 1.54	37.56 ± 6.15
PUB$_{0.6}$	10.78 ± 2.19	39.64 ± 3.98
PUB$_1$	9.44 ± 0.45	42.37 ± 7.54
PU$\alpha_{0.2}$	10.32 ± 1.86	40.93 ± 5.14
PU$\alpha_{0.6}$	10.83 ± 1.79	48.04 ± 7.17
PUα_1	11.53 ± 1.04	52.04 ± 4.02
PUN$_{0.2}$	8.74 ± 0.03	48.76 ± 3.86
PUN$_{0.6}$	9.61 ± 0.19	52.69 ± 1.36
PUN$_1$	5.62 ± 0.47	46.21 ± 4.86

isocyanate was considered the gel time.[34] The average gel times of PUB and PUα were slightly longer than that of neat foam. This was probably attributed to the low reactivity of bamboo fibers, which hindered the reaction between polyols and isocyanate. The rise times of PUB and PUα gradually increased with increasing biomass content. This was ascribed to the high viscosity of mixtures containing bamboo fibers, which could undermine the foaming reaction.[35] From Table 1, the average gel time of PUN was shorter than that of PU_0. Our previous work evidenced that nanocellulose could react with isocyanate, resulting in the enhancement of the forming process.[31] It was reported that dimethylformamide (DMF), used as a diffuser, could promote the reaction between polyols and isocyanate.[36] The rise time of PUN increased first and then decreased with increasing nanocellulose fiber content, which probably corresponded to the change in the viscosity of the mixture. The addition of nannocellulose could change the viscosity of the mixture remarkably and probably result in agglomeration.[31]

2.3. FTIR of Biofoam Absorbents. The FTIR spectra of resulting biofoam adsorbents are shown in Figure 3. The bands
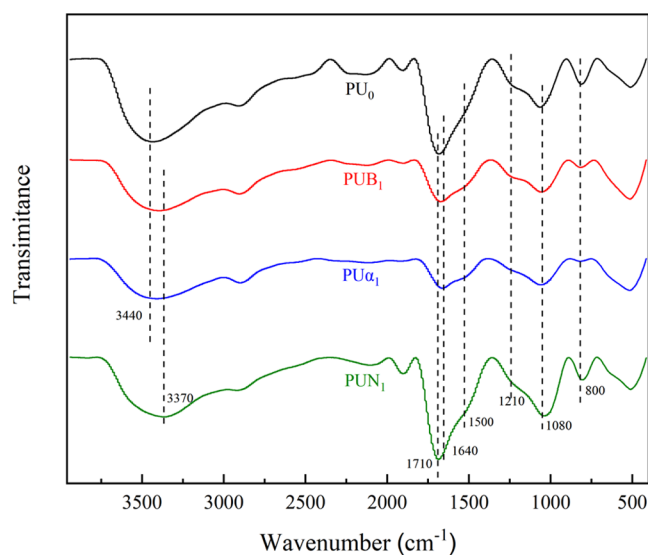

Figure 3. FTIR spectra of PU_0, PUB_1, $PU\alpha_1$, and PUN_1.

at 3440 cm^{-1} were found in all biofoam adsorbent samples. These were associated with the N−H stretching of urethane linkage in PU foams with the bamboo fiber source segment region.[37] The peaks at 3440 cm^{-1} red shifted to 3370 cm^{-1} in PUN_1, which may be due to graft polymerization of nanocellulose with numerous hydroxyl groups.[38] The peak at 1710 cm^{-1} appeared in biofoam adsorbents, which was ascribed to the stretching vibration of C=O from the aldehyde or saturated chain.[39] It demonstrated the reaction between bamboo fiber sources and isocyanate groups. The peak at 1640 cm^{-1} from the bending vibration of H−O−H confirmed the existence of unreacted water in the foaming process.[39] The presence of isocyanurate was indicated by absorption characteristic peaks of the N−H signal at 1500, 1210, 1080, and 800 cm^{-1}, which was formed by the undesired reactions between isocyanate and urethane groups.[40] Comprehensively, these findings indicated that biofoam adsorbents were formed by the reaction between bamboo fiber sources and the PU matrix.

2.4. SEM of Biofoam Adsorbents. The scanning electron microscopy (SEM) images of the resulting biofoam adsorbents are shown in Figure 4. The straight bamboo fiber complexes were wrapped and interspersed in the PU foam matrix (Figure 4a). However, the α-cellulose fibers in the PU foam matrix tended to be twisted, and the fiber complexes were unwrapped (Figure 4b). Most of the lignin and hemicellulose in bamboo fibers were removed by alkali and bleaching treatment, resulting in single and twisted α-cellulose fibers with high specific surface areas, as compared with the bamboo fiber. It may be beneficial to the excellent adsorption effect at the early adsorption stage.[41] From Figure 4c, numerous spheres were observed in the PU matrix. These particles were formed by a huge amount of nucleation points between nanocellulose and DMF, which probably resulted in a large number of adsorption sites.[42,43]

2.5. TG and DTG of Biofoam Adsorbents. The thermal properties of biofoam adsorbents were studied by thermogravimetric and differential thermogravimetric (TG and DTG) analyses (Figure 5). The pyrolysis of biofoam adsorbents was divided into three weight loss stages. The first decomposition stage was in the range of 25−210 °C, which was mainly involved in the dehydration of biofoam adsorbents.[44] The main weight loss peak was between 210 and 370 °C. This was characteristic of the urethane bond of cellulose and hemicellulose decomposition, followed by chain scission of the polyol backbone.[45] The final degradation region, above 550 °C, was mainly the decomposition of ash formed by biofoam adsorbents.[46]

PUB_1 reached the maximum loss rate in the range of 210−370 °C, which was ascribed to the decomposition of hemicellulose in the bamboo fiber.[47] All main thermal degradation temperatures (210−370 °C) of biofoam adsorbents were higher than that of PU_0, suggesting that the thermal stability of biofoam adsorbents was higher than that of neat foam. The mass loss rate peak at 400 °C of PU_0 foam was higher than that of biofoam adsorbents. This was mainly attributed to bamboo fiber sources delaying the decomposition of PU_0 by forming a protective layer.[48] By removing noncellulose and improving cellulose crystallinity, the residual mass of biofoam adsorbents was increased at 770 °C. This could be ascribed to the biochar obtained from the high crystallinity of cellulose.[49] Therefore, the thermal stability of biofoam adsorbents with α-cellulose and nanocellulose fibers were improved due to the cross-links between high-crystallinity cellulose and the polyurethane system.[31]

2.6. Adsorption of MB and Cu(II). *2.6.1. Effect of Contact Time.* The contact time was an important factor to tell the time required for the maximum removal of dyes from water solution.[50] The relationship between contact time and the cationic adsorption efficiency of biofoam adsorbents is shown in Figure 6. As shown in Figure 6a, the MB removal efficiency of PUB_1 was increased from 45.12 to 71.16% within 60 h. It could be observed that adsorption was not fully saturated at 60 h. The unsaturated adsorption of PUB_1 was ascribed to the unexposed adsorption sites of hemicellulose and lignin.[51] The MB removal efficiencies of $PU\alpha_1$ and PUN_1 increased first and then stabilized at 73.94 and 95.52%, respectively, as the contact time reached 60 h. These results indicated that PUN_1 had the maximum adsorption capacity for MB, which was ascribed to the high specific surface area and a large number of exposed hydroxyl groups on the surface of nanocellulose.[52] All of the adsorption efficiencies of biofoam adsorbents were greater than
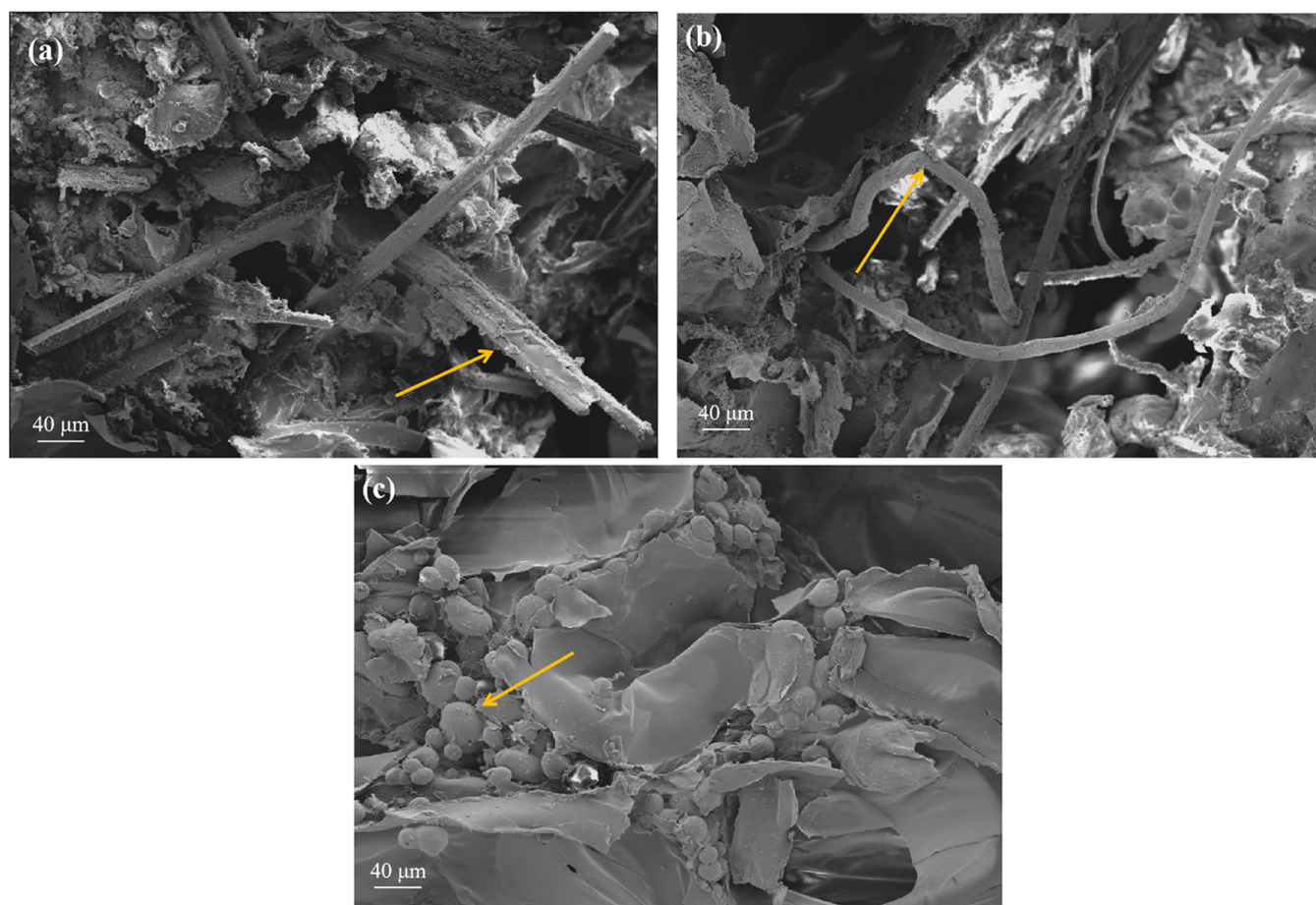
Figure 4. SEM images of biofoam adsorbents: (a) PUB_1, (b) $PU\alpha_1$, and (c) PUN_1.
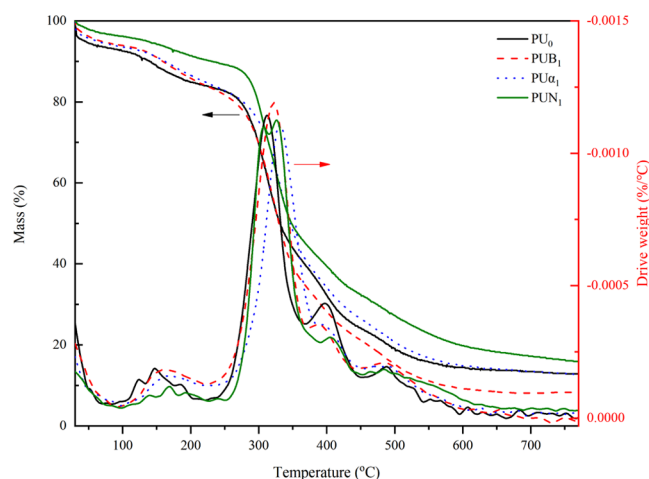

Figure 5. TG and DTG curves of biofoam adsorbents.

that of PU_0, which was ascribed to the pure foam mainly acting as a matrix and having poor adsorption capacity.[53]

Figure 6b shows the Cu(II) removal by biofoam adsorbents. Since PU_0 did not exhibit any adsorption capacity on Cu(II), it had not been included in this work. Cu(II) removal was found to increase to 100% for PUB_1 within 24 h, which was remarkably higher than that of PUN_1 and $PU\alpha_1$. It was due to the good adsorption potential of hemicellulose and lignin in the bamboo fiber.[52] Cu(II) removal reached 95.16% for $PU\alpha_1$ within 24 h and then decreased with increasing time, which

was probably ascribed to all of the active sites on α-cellulose being saturated with Cu(II).[54] About 100% Cu(II) removal was obtained by PUN_1 within 48 h, which was probably ascribed to the huge specific surface of PUN_1 with a negative charge to attract Cu(II).[3] The 100% Cu(II) removal by PUB_1 within 24 h suggested that low-cost PUB_1 could be used for the adsorption and recovery of Cu(II) from wastewater.

2.6.2. Effect of pH. Figure 7 illustrates the removal of MB and Cu(II) by biofoam adsorbents with regard to pH. From Figure 7a, it was worth noting that PUN_1 had a stable and efficient adsorption capacity (>2.15 mg/g) for MB. This phenomenon was partially attributed to the hydrogen bonding formed between MB and PUN_1 that has a large number of −OH groups.[5] Furthermore, sulfuric acid hydrolysis used to produce nanocellulose could introduce negatively charged sulfate ester.[55] This could contribute to attracting positive charged cationics. By increasing the pH from 3 to 11, the MB adsorption capacity of PUB_1 increased from 0.48 to 2.34 mg/g with 98.61% MB removal efficiency and that of $PU\alpha_1$ increased from 0.50 to 2.32 mg/g. The pH dependence of PUB_1 and $PU\alpha_1$ was due to PUB_1 and $PU\alpha_1$ behaving differently to charge behaviors at different pH levels to react with positively charged MB.[1]

Cu(II) precipitates when the pH is above 7. Therefore, the adsorption of Cu(II) was conducted in the neutral and acid environments in this work. From Figure 7b, the Cu(II) adsorption capacities of biofoam adsorbents increased with increasing pH from 3 to 7. The intense competition between H^+ and Cu(II) for active binding sites on the adsorbent would
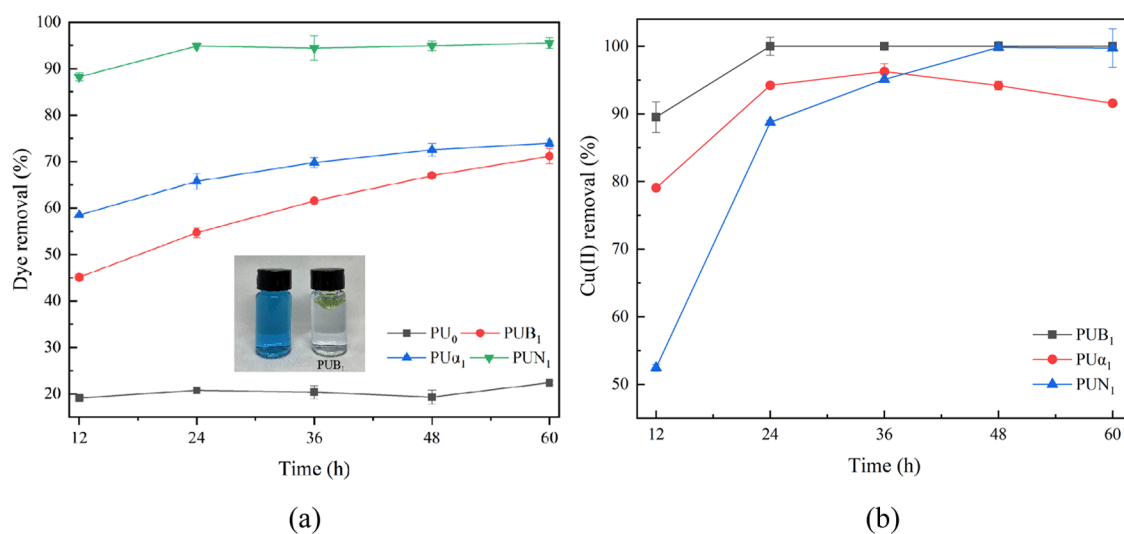
(a)

(b)

Figure 6. Effects of contact time on the removal of cationics ((a) MB, (b) Cu(II)) by biofoam adsorbents (pH = 7; T = 25 °C; (a) initial content = 25 mg/L; (b) initial content = 15 mg/L).

(a)

(b)

(c)

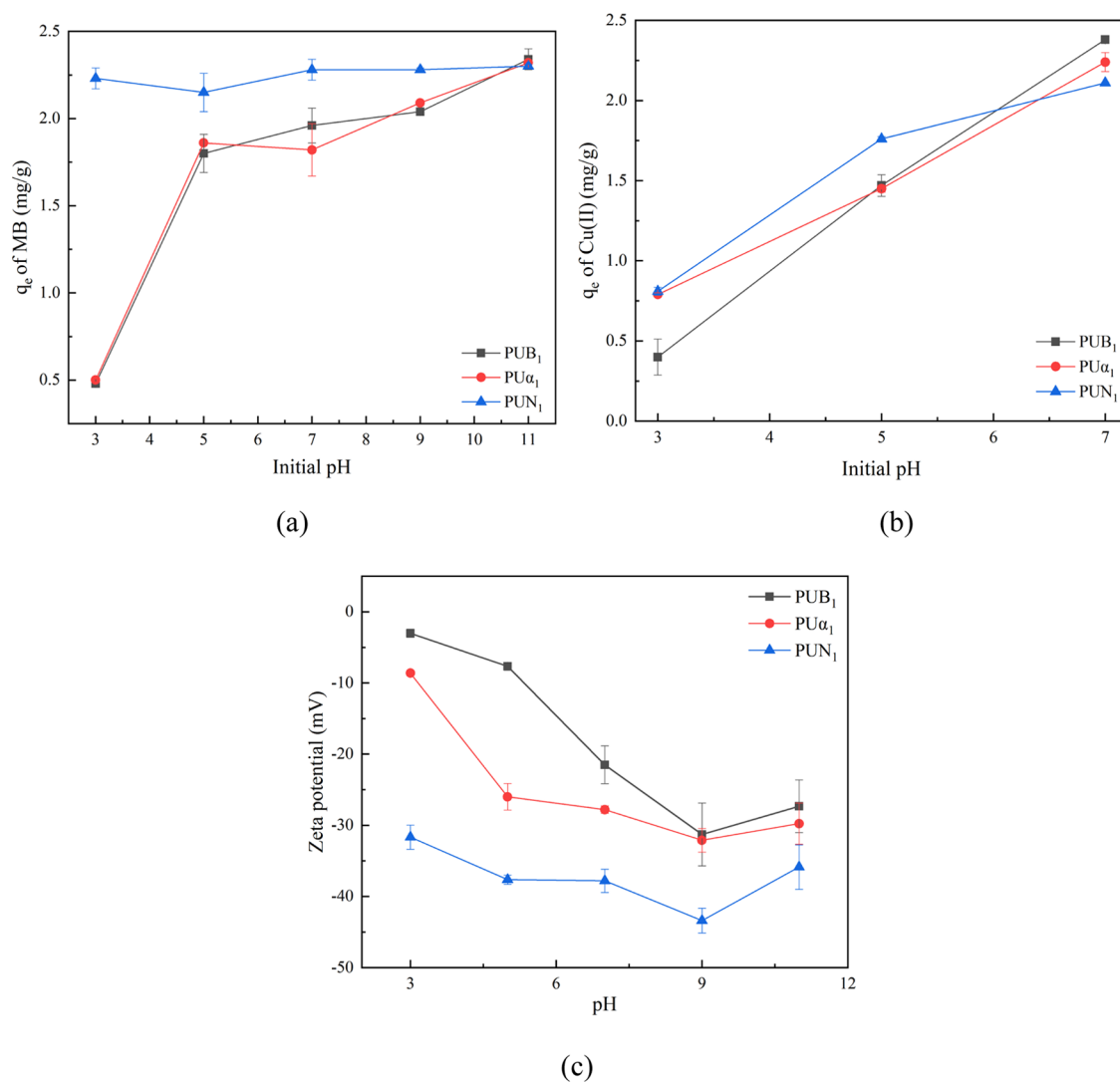**Figure 7.** Effects of pH on the adsorption efficiencies of cationic pollutants ((a) MB; (b) Cu(II)) (initial content = 15 mg/L; T = 25 °C); (c) ζ potential of biofoam adsorbents.
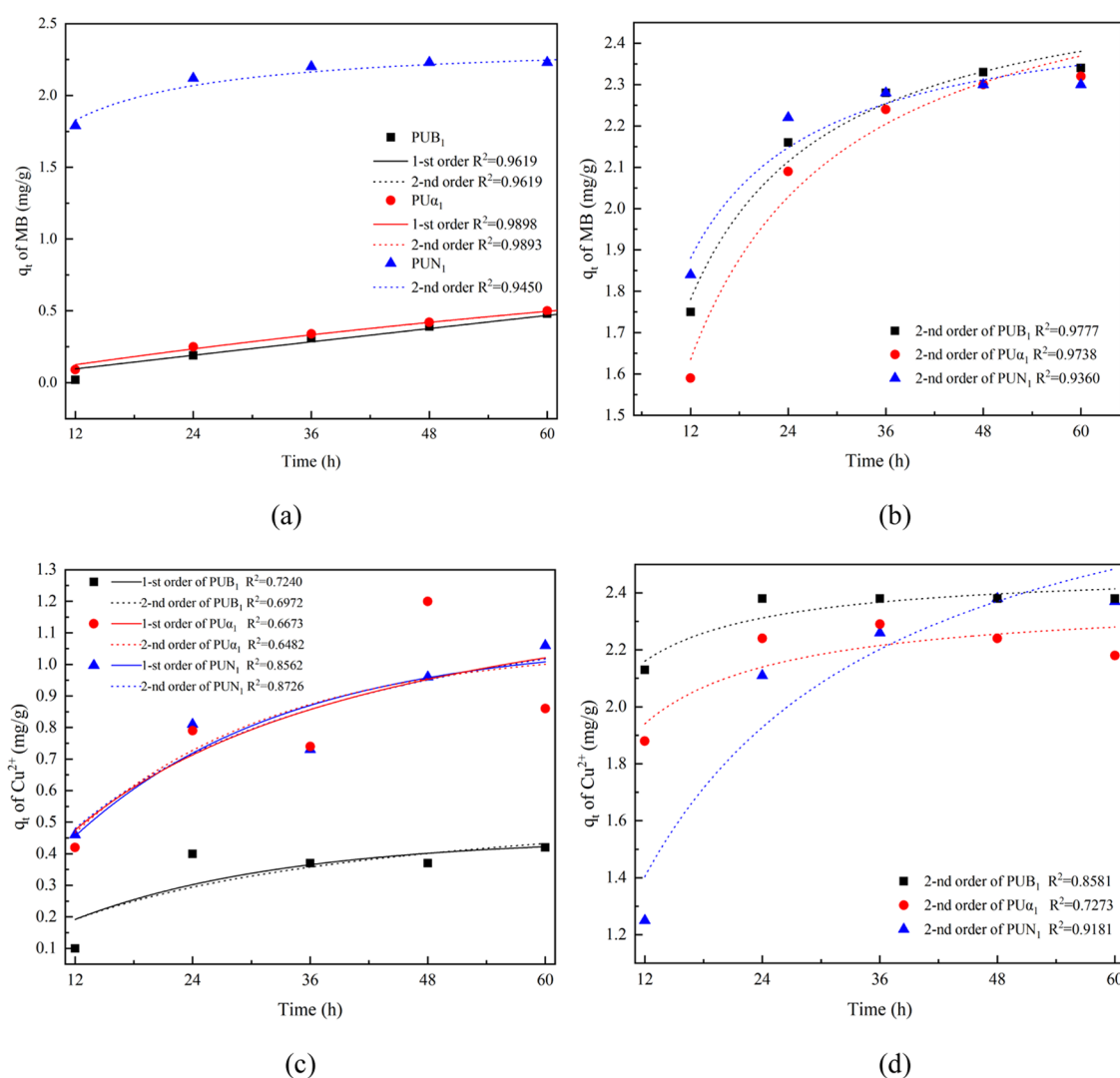
Figure 8. Kinetic models for cationic pollutant adsorption ((a) pH = 3 and (b) pH = 11 for MB; (c) pH = 3 and (d) pH = 7 for Cu(II)) by biofoam adsorbents (initial content = 15 mg/L; T = 25 °C).

Table 2. Kinetic Parameters for MB (pH = 11) and Cu(II) (pH = 7) Adsorption by Biofoam Adsorbents

model	parameters	pH	adsorbate (MB)			adsorbate (Cu(II))		
			PUB_1	$PU\alpha_1$	PUN_1	PUB_1	$PU\alpha_1$	PUN_1
first-order kinetic	k_1 (g/(mg·h))		N/A	N/A	N/A	N/A	N/A	N/A
	q_{exp} (mg/g)	11 (MB)						
	q_{cal} (mg/g)	7 (Cu(II))						
	R^2							
second-order kinetic	k_1 (g/(mg·h))		0.00103	0.0100	N/A	0.0463	0.0485	0.0459
	q_{exp} (mg/g)	3 (MB)	0.4751	0.5022		0.4247	0.8635	1.0641
	q_{cal} (mg/g)	3 (Cu(II))	7.8115	1.099		0.4504	1.0584	1.0766
	R^2		0.9619	0.9898		0.7240	0.6673	0.8562
	k_2 (g/(mg·h))		0.0698	0.0494	0.1007	0.2218	0.1529	0.0245
	q_{exp} (mg/g)	11 (MB)	2.5994	2.6689	2.5063	2.4868	2.38415	3.07653
	q_{cal} (mg/g)	7 (Cu(II))	2.3478	2.3392	2.3078	2.3810	2.1800	2.3743
	R^2		0.9777	0.9738	0.9360	0.8581	0.7273	0.9181
	k_2 (g/(mg·h))		0.0001	0.0030	0.1149	0.0579	0.0304	0.0289
	q_{exp} (mg/g)	3 (MB)	0.4751	0.5022	2.3041	0.4247	0.8635	1.0641
	q_{cal} (mg/g)	3 (Cu(II))	16.0754	1.9228	2.3837	0.6301	1.4128	1.4333
	R^2		0.9619	0.9893	0.9450	0.6972	0.6482	0.8726

be weakened when the pH was increased.[56] The maximum Cu(II) adsorption capacity of PUB_1 was 2.38 mg/g, which was greater than those of PUN_1 (2.11 mg/g) and $PU\alpha_1$ (2.24 mg/g). Cu(II) adsorption by the bamboo fiber was attributed to
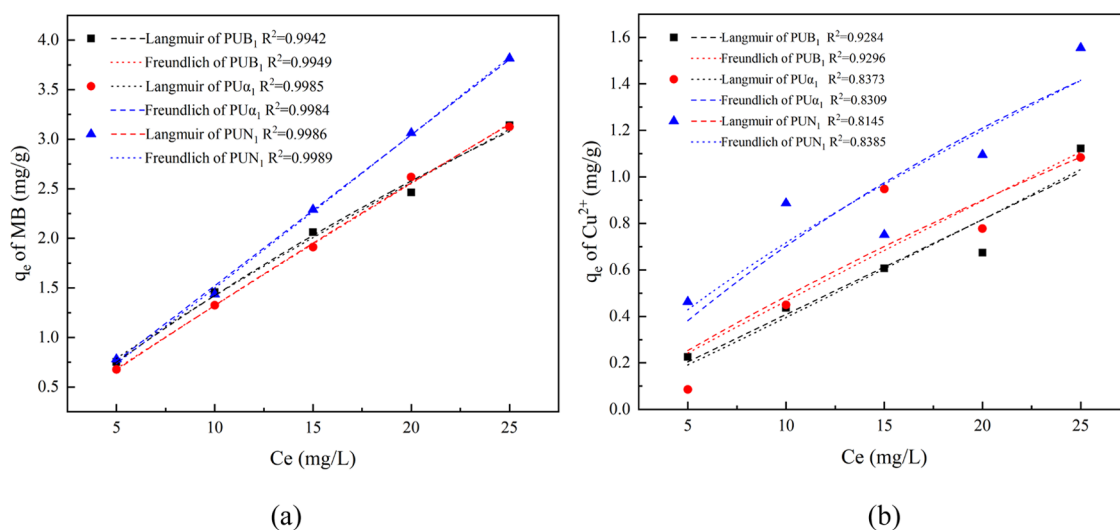
Figure 9. Adsorption isotherms for cationic pollutant adsorption ((a) MB; (b) Cu(II)) by biofoam adsorbents (T = 25 °C; (a) pH = 7; (b) pH = 3).

Table 3. Isotherm Parameters for MB and Cu(II) (pH = 7) Adsorption by Biofoam Adsorbents

model	parameters	adsorbate (MB)			adsorbate (Cu(II))		
		PUB$_1$	PUα_1	PUN$_1$	PUB$_1$	PUα_1	PUN$_1$
Langmuir isotherm	K_L (L/g)	0.012	0.004	0.002	0.013	0.009	0.019
	q_m (mg/g)	13.69	38.53	93.42	7.05	6.11	4.39
	R^2	0.9942	0.9985	0.9986	0.9284	0.8373	0.8145
	R_L	0 < R_L < 1					
Freundlich isotherm	K_f	0.201	0.149	0.142	0.035	0.053	0.130
	n	1.176	1.053	0.978	0.954	1.058	1.348
	R^2	0.9949	0.9984	0.9989	0.9296	0.8309	0.8385
Gibbs free energy model	$\Delta G°$	11.04 kJ/mol	13.94 kJ/mol	15.66 kJ/mol	10.74 kJ/mol	11.78 kJ/mol	9.82 kJ/mol

the hydrogen bonding between Cu(II) and hydroxyl groups (i.e., −Cu(II) and −OH).[57] The high adsorption performance of PUN$_1$ toward Cu(II) suggested that PUN$_1$ could be used as a Cu(II) adsorbent in wastewater.

Figure 7c shows the pH-dependent ζ-potentials of biofoam adsorbents. The biofoam adsorbents had a negative charge at pH from 3 to 11. The negative charge amount of biofoam adsorbents increased at pH from 3 to 9 and then decreased at pH from 9 to 11. This result indicated that the maximum adsorption capacities toward cationic pollutants were obtained at pH 9. Furthermore, PUN$_1$ had the highest adsorption capacities at acid environment toward MB and Cu(II) for its largest negative charge, as shown in Figure 7c.[58]

2.6.3. Adsorption Kinetics. The adsorption kinetics of MB and Cu(II) by biofoam adsorbents are shown in Figure 8 and Table 2. To predict the adsorption tendencies and the cationic pollutants' removal rates from wastewater, kinetic investigations were evaluated by the pseudo-first-order and pseudo-second-order models. It was observed from Figure 8a that the MB adsorption processes by PUB$_1$ and PUα_1 were fitted well using pseudo-first-order kinetics at pH 3. The correlation coefficients (R^2) were 0.96 and 0.99, respectively (Table 2). The pseudo-first-order kinetics indicated that the adsorption of MB by PUB$_1$ and PUα_1 was mainly controlled by the diffusion process.[43,51] This result was probably due to the low MB capture rate by hydroxyl groups of PUB$_1$ and PUα_1 in the initial adsorption stage at pH 3.[59] The pseudo-second-order kinetics was fitted well to all adsorption processes at pH 11

(Figure 8b). The R^2 values were 0.98, 0.97, and 0.94 for PUB$_1$, PUα_1, and PUN$_1$, respectively (Table 2). The results indicated the pseudo-second-order kinetics was better to describe the adsorption process of MB than the pseudo-first-order kinetics. It suggested that the removal of MB by PUB$_1$, PUα_1, and PUN$_1$ samples was controlled by chemical adsorption.[51,60,61]

From Figure 8c, the Cu(II) adsorption processes by PUB$_1$ and PUα_1 were fitted well using pseudo-first-order kinetics, while the one adsorbed by PUN$_1$ was fitted well using pseudo-second-order kinetics at pH 3. The pseudo-second-order kinetics was found to fit better to all adsorption processes by biofoam adsorbents at pH 7. Therefore, it was inferred that the adsorption of Cu(II) by PUB$_1$, PUα_1, and PUN$_1$ samples was controlled by chemical adsorption.[56,62] This adsorption process included the sharing and exchanging of electrons between the adsorbent and Cu(II).[56,63]

2.6.4. Adsorption Isotherms. Adsorption isotherms on MB and Cu(II) of PUB$_1$, PUα_1, and PUN$_1$ were carried out to determine the adsorption capacities and interactive behaviors between the adsorbent and the adsorbate (Figure 9 and Table 3). The MB adsorption isotherm of PUα_1 was fitted well by the Langmuir model (R^2 > 0.99). This result indicated that the adsorption of MB occurred by hydrogen bonding between the hydroxyl groups and MB molecule surface binding sites to form a monolayer.[56,63] From Table 3, the R_L values for all pollutants were in the range of 0−1, which indicated that the adsorption or complexation processes were favorable.[7] The MB adsorption isotherm of PUB$_1$ and PUN$_1$ was fitted well by

the Freundlich model (Table 3), suggesting that the adsorption of MB occurred on the heterogeneous surface by multilayer adsorption.[4,51,64] Hence, the adsorption process of $PU\alpha_1$ was a monolayer, and the adsorption of MB by PUB_1 and PUN_1 was multilayer adsorption. Interestingly, similar results could be observed in other reported literature works.[4,51,56,64]

The Cu(II) adsorption isotherms by PUB_1 and PUN_1 were fitted well by the Langmuir model ($R^2 > 0.84$), indicating that the active adsorption sites were homogeneously distributed on the surface of PUB_1 and PUN_1 by monolayer adsorption.[50] In contrast, the Cu(II) adsorption isotherm of $PU\alpha_1$ was fitted well by the Freundlich model ($R^2 > 0.84$). In this model, the $1/n$ values of PUB_1 and $PU\alpha_1$ were below 1, indicating that the adsorption of Cu(II) occurred on heterogeneous binding sites by multilayer adsorption.[64,65] Moreover, similar results were observed from Cu(II) adsorption by nanocellulose-based polyethylenimine aerogel, functionalized paper, and polyampholyte hydrogel.[50,64,65]

From Table 3, the MB and Cu(II) adsorption Gibbs free energies for PUB_1, $PU\alpha_1$, and PUN_1 were 11.04, 13.94, and 15.66 and 10.74, 11.78, and 9.82 kJ/mol, respectively. The Gibbs free energy confirmed the powerful adsorption ability of biofoam adsorbents to remove MB and Cu(II).[4] This evidenced the high speed of MB and Cu(II) adsorption by biofoam adsorbents.[65]

The MB and Cu(II) maximum adsorption capacities of biofoam adsorbents of PUB_1, $PU\alpha_1$, and PUN_1 calculated by the Langmuir model were 13.69, 38.53, and 93.42 and 7.05, 6.11, and 4.39 mg/g, respectively. The maximum MB adsorption capacity of PUN_1 was higher than the values reported in the literature works, such as tamarind fruit shell, bamboo shoot skin, and nanocellulose hydrogel (Table 4).[59,66,67] The Cu(II) removal efficiency of PUB_1 was better than those of citric acid-modified barley straw and raw pomegranate peel biosorbent (Table 4).[68,69]

Table 4. Comparison of Adsorption Capacities of Biofoam Adsorbents with Literature Works

adsorbents	MB or Cu(II) adsorption capacity	ref
tamarind fruit shell	1.98 mg/g (MB)	59
bamboo shoot skin	29.88 mg/g (MB)	66
nanocellulose hydrogel	47.13 mg/g (MB)	67
PUB_1, $PU\alpha_1$, and PUN_1	13.69, 38.53, and 93.42 mg/g (MB)	this work
EDTA-modified cellulose filter paper	93.00% (Cu(II))	63
citric acid-modified barley straw	88.10% (Cu(II))	68
raw pomegranate peel biosorbent	88.99% (Cu(II))	69
PUB_1	100.00% (Cu(II))	this work

2.7. Desorption and Reusability. The reusability of biofoam adsorbents is shown in Figure 10. The MB adsorption efficiencies decreased with increasing recycle time. After the first recycle, PUB_1 and PUN_1 retained excellent MB removal efficiencies. These were 77.66 and 88.77%, respectively. However, that of $PU\alpha_1$ was only 42.55%. This result indicated that $PU\alpha_1$ had very poor reusability. After the fifth recycle, PUN_1 still could remove about 61.25% of MB dye. However, the MB removal efficiencies were only around 23.38 and 16.71% of PUB_1 and $PU\alpha_1$, suggesting that PUN_1 had good
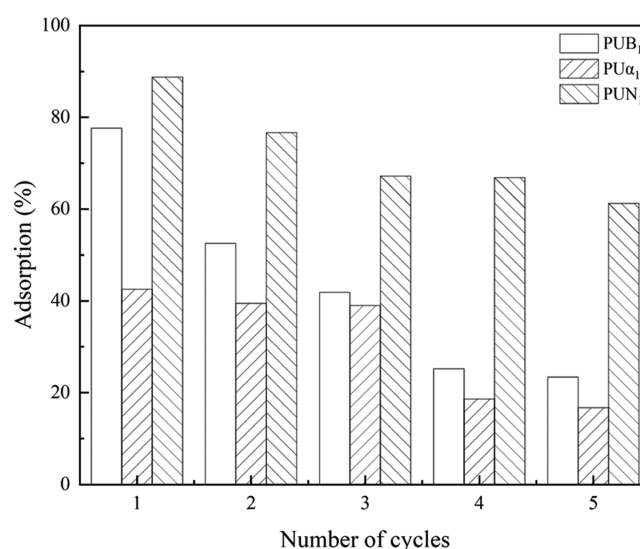

Figure 10. Recycling of the biofoam adsorbents for the removal of MB (initial content = 25 mg/L; pH = 7; T = 25 °C).

potential to be used as a reusable adsorbent for the treatment of MB in wastewater.

2.8. Adsorption Mechanism. As shown in Figure 11a, the wide bands at around 3440 cm^{-1} of PUB_1 and PUN_1 were due to O−H and N−H vibrations.[29] These bands weakened after adsorption MB, indicating that the hydroxyl groups played important roles in hydrogen bond formation in the MB adsorption process.[70] Besides, it could be seen that the peak at 1390 cm^{-1} was enhanced. This peak was assigned to the C−N stretching vibration of MB, which proved that the MB molecules were adsorbed onto biofoam adsorbents.[71] From Figure 11b, there was an obvious decrease in the intensity at 3440 cm^{-1} after Cu(II) adsorption. This peak was assigned to the hydroxyl groups of bamboo fiber sources. This change could infer that the hydroxyl groups were the main adsorption sites in the Cu(II) adsorption process.[72]

Based on the FTIR analysis, Figure 12 shows a schematic illustration of the adsorption mechanism of MB and Cu(II). The hydrogen-bonding interactions occurred between hydroxyl groups of biofoam adsorbents and cationic pollutants (MB and Cu(II)). Moreover, the $n-\pi$ interaction came from delocalization of the lone pair electron of O atoms into the π orbital of the MB dye aromatic rings.[73] These interactions were effective in enhancing the adsorption of MB and Cu(II).

3. CONCLUSIONS

Biofoam adsorbents were produced by incorporating bamboo waste sources, i.e., bamboo fiber, bamboo α-cellulose fiber, and bamboo nanocellulose fiber, into a polyurethane (PU) foam matrix. The resulting biofoam adsorbents had excellent adsorption performances in removing low-concentration cationic pollutants (methylene blue and Cu(II)). The hydroxyl groups of bamboo fiber sources reacted with isosyanate groups in the resulting biofoam adsorbents. The biofoam adsorbents with bamboo fiber sources had better thermal stability than neat foam. The maximum MB removal efficiency of PUN_1 (PU with 1 g of nanocellulose) was 95.52% and the maximum Cu(II) removal efficiency of PUB_1 (PU with 1 g of bamboo fiber) was 100% at pH 7. The adsorption of MB and Cu(II) was well described by pseudo-second-order kinetics. In addition, PUN_1 had excellent recyclability that could keep
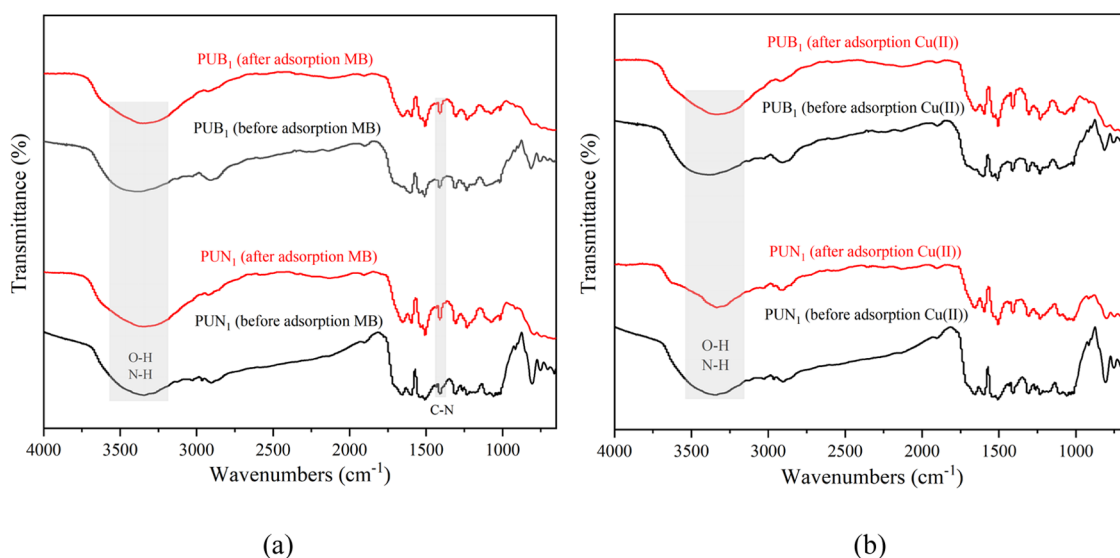
Figure 11. FTIR spectra of PUB$_1$ and PUN$_1$ before and after adsorption of MB (a) and Cu(II) (b).
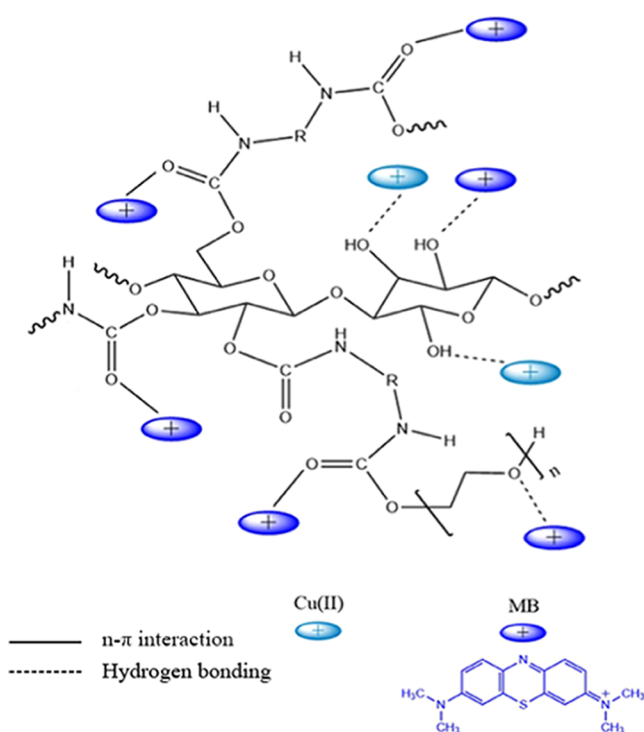

Figure 12. Schematic illustration of the adsorption mechanism.

61.25% MB removal after five recycles. PUN$_1$ was effective in removing cationic pollutants from aqueous solutions, which could be used as a reusable adsorbent for the treatment of MB in wastewater. The novelty of this work was that low-cost PUB$_1$ prepared in a simple process had outstanding performance of 100% Cu(II) removal. It suggested that PUB$_1$ derived from bamboo waste is a good candidate to be used as a promising biosorbent for the adsorption and separation of Cu(II) from wastewater.

4. EXPERIMENTAL SECTION

4.1. Materials. Bamboo fiber sources, i.e., bamboo fiber, bamboo α-cellulose fiber, and bamboo nanocellulose fiber,

were prepared from Moso bamboo (*Phyllostachys heterocycla* cv. *pubescens*) waste according to our previous work.[28]

Chemicals, including toluene, ethanol, glacial acetic acid, sodium chlorite, sulfuric acid (H$_2$SO$_4$, 98 wt %), polyethylene glycol 400, dimethicone, *N,N*-dimethylformamide (DMF), and sodium hydroxide, were purchased from Kelong Chemical Co. Ltd. (Chengdu, Sichuan, China). Polyether polyol (330 N) was provided by Dongda Wenlong Chemical Co. Ltd. (Guangzhou, Guangdong, China). The silicone foam stabilizer was purchased from Hongming Chemical Co. Ltd. (Jining, Shandong, China), and the opening agent was purchased from Lanxin Chemical Co. Ltd. (Shanghai, China). Isocyanate was purchased from Tairong Chemical Trading Co. Ltd. (Guangzhou, Guangdong, China). All chemicals were used without further purification.

4.2. Preparation of Biofoam Adsorbents. The prepolymer was prepared by mixing polyethylene glycol 400, dimethicone, water, polyether polyol, and the silicone foam stabilizer in a beaker (100 mL) equipped with a motor-driven stirrer. The biomass sources were dissolved in DMF (10 v/v) by sonication (150 W) for 15 min. After the biomass fibers (bamboo fiber, α-cellulose, and nanocellulose) were evenly dispersed in DMF, the DMF mixture was mixed with the prepolymer, followed by stirring for 10 min. Isocyanate was added to the mixture and stirred well until the mixture became white, and then, it was injected into a plastic cylindrical mold (100 mL) at 25 °C for 24 h. The biofoam adsorbent without biomass fiber was labeled as PU$_0$, and the ones having bamboo fiber, α-cellulose fiber, and nanocellulose fiber (0.2, 0.6, and 1 g) were named as PUB$_{0.2}$, PUB$_{0.6}$, PUB$_1$, PU$\alpha_{0.2}$, PU$\alpha_{0.6}$, PUα_1, PUN$_{0.2}$, PUN$_{0.6}$, and PUN$_1$, respectively.

4.3. Characterization of Bamboo Fiber Sources. FTIR analysis was performed on a Nicolet IS10 spectrometer (Thermo Fisher Scientific, MA). A small quantity of the sample was covered flatwise on the detection window. Each biomass fiber was analyzed in the range of resolution from 400 to 4000 cm^{-1} with a spectral resolution of 4 cm^{-1}, and a total of 32 scans were collected.

4.4. Characterization of Biofoam Adsorbents. The FTIR analysis of the biofoam adsorbents was performed on a Nicolet IS10 spectrometer (Thermo Fisher Scientific, MA).

The morphologies of the biofoam adsorbents were examined using scanning electron microscopy (SEM, JSM-6110 LV, Tokyo, Japan). Thermogravimetric and differential thermogravimetric (TG/DTG) analyses of biofoam adsorbents were conducted with a NETZSCH STA 449 F5/F3 Jupiter (NETZSCH-Gerätebau GmbH, Selb, Germany) to simultaneously obtain thermogravimetric data. Each sample (approximately 5 mg) was analyzed at 30−800 °C with a constant heating rate of 10 °C/min under a flow of 40 mL/min of nitrogen. ζ-potentials of biofoam adsorbents at different pH levels were determined by a Zetasizer Ultra (Malvern Panalytical, Shanghai Specter Instrument System Co., Ltd., China).

4.5. Absorption Studies. Biofoam adsorbents were applied to remove cationic pollutants (MB and Cu(II)) from aqueous solutions. The biofoam adsorbents were cut into samples of 0.16 g each and were placed into cationic pollutant aqueous solutions (25 mL, 5 to 25 mg/L) for 60 h. The aqueous solutions containing 25 mg/L cationic pollutants were adjusted to the desired pH from 3.0 to 11.0 by adding 0.1 mol/L HCl and/or 0.1 mol/L NaOH. Moreover, the adsorption kinetics and isotherms were studied at different times (12−60 h) and initial concentrations (5−25 mg/L). The adsorption capacity of biofoam adsorbents toward MB was estimated by calculating the change between initial and residual MB concentrations using a UV spectrophotometer (UV-4802H, Unico, Shanghai, China) at 664 nm. The concentration of Cu(II) was determined using an AA-6300 atomic absorption spectrophotometer with an air−acetylene burner (AAS, Shimadzu, Japan). The cationic pollutant adsorption capacities (q_e) were calculated according to eq 1

$$q_e = \frac{C_0 - C_e}{m} \times V \tag{1}$$

where C_0 (mg/L) and C_e (mg/L) are the initial and residual cationic pollutant concentrations, respectively, V (L) is the volume of the cationic pollutant aqueous solution, and m (mg) is the weight of biofoam adsorbents.

4.5.1. Adsorption Kinetics and Isotherms. The kinetic data of cationic pollutants adsorbed by biofoam adsorbents were fitted using pseudo-first-order (eq 2) and pseudo-second-order (eq 3) models.

$$\ln(q_e - q_t) = \ln q_e - k_1 t \tag{2}$$

$$\frac{t}{q_t} = \frac{1}{k_2 q_e^2} + \frac{t}{q_e} \tag{3}$$

where t is the contact time (h), q_e is the adsorbed concentration of cationic pollutants (mg/g) at equilibrium, q_t is the equilibrium concentration of cationic pollutants (mg/g) at time t, and k_1 and k_2 are rate constants (g/(mg·h)).

The adsorption kinetic data of cationic pollutants adsorbed by biofoam adsorbents were fitted using Langmuir and Freundlich isotherm models (eq 4 and 5).

$$\frac{C_e}{q_e} = \frac{1}{K_L q_m} + \frac{1}{q_m} C_e \tag{4}$$

$$\ln q_e = \ln K_f + \frac{1}{n} \ln C_e \tag{5}$$

where q_m and k_L represent the maximum adsorption capacity of the adsorbents and the constant energy related to the heat of adsorption, respectively, C_e (mg/L) is the concentration of the adsorbate in the liquid phase at equilibrium, and q_e (mg/g) is the amount of the adsorbate in the solid phase at equilibrium. K_f (mg/g) (L/mg)$^{1/n}$ indicates the adsorption capacity, and n reflects the intensity of adsorption according to the Freundlich theory, which gives an idea of the favourability of adsorption. A value of $1/n$ between 0 and 1 indicates favorable and heterogeneous adsorption.

The essential characteristic of the Langmuir isotherm on the nature can be assessed by a dimensionless equilibrium parameter (eq 6)

$$R_L = \frac{1}{1 + K_L C_0} \tag{6}$$

where R_L is a dimensionless equilibrium parameter or the separation factor and C_0 is the initial concentration of the adsorbate solution (mg/L). The value of R_L denotes the adsorption nature to be unfavorable ($R_L > 1$), favorable ($0 < R_L < 1$), irreversible ($R_L = 0$), or linear ($R_L = 1$).

4.5.2. Adsorption Thermodynamics of Temperature. The thermodynamics data of MB adsorbed by biofoam adsorbents was fitted by the Gibbs free energy model (eq 7).

$$\Delta G° = -RT \ln K_L \tag{7}$$

where $\Delta G°$ is the Gibbs free energy, R is the universal gas constant (8.314 J/(mol K)), T (K) is the absolute temperature ($T = 298$ K), and K_L (L/g) is the Langmuir constant.

4.6. Regeneration of Biofoam Adsorbents. After the adsorption of cationic pollutants, the biofoam adsorbents were added to 90% ethanol solution (100 mL) in a thermostatic water bath shaker with a speed of 80 rpm at 25 °C for 2 h. Afterward, the biofoam adsorbents were filtered from the solution and washed with distilled water several times. The recycled biofoam adsorbents were subjected to the next adsorption−desorption cycle.

■ AUTHOR INFORMATION

Corresponding Authors

Feng Li − *Landscape Architecture School, Chengdu Agricultural College, Chengdu, Sichuan 611130, China;* Email: Li_feng2016@126.com

Xingyan Huang − *College of Forestry, Sichuan Agricultural University, Chengdu, Sichuan 611130, China;* ● orcid.org/0000-0001-8622-5320; Email: hxy@sicau.edu.cn

Authors

Chongpeng Qiu − *College of Forestry, Sichuan Agricultural University, Chengdu, Sichuan 611130, China*

Xuelun Zhang − *College of Forestry, Sichuan Agricultural University, Chengdu, Sichuan 611130, China*

You Zhang − *College of Forestry, Sichuan Agricultural University, Chengdu, Sichuan 611130, China*

Qi Tang − *College of Forestry, Sichuan Agricultural University, Chengdu, Sichuan 611130, China*

Zihui Yuan − *College of Forestry, Sichuan Agricultural University, Chengdu, Sichuan 611130, China*

Cornelis F. De Hoop − *School of Renewable Natural Resources, Louisiana State University Agricultural Center, Baton Rouge, Louisiana 70803, United States*

Jiwen Cao − *College of Forestry, Sichuan Agricultural University, Chengdu, Sichuan 611130, China*

Shilin Hao − *College of Forestry, Sichuan Agricultural University, Chengdu, Sichuan 611130, China*

Ting Liang − *College of Forestry, Sichuan Agricultural University, Chengdu, Sichuan 611130, China*

Complete contact information is available at:

https://pubs.acs.org/10.1021/acsomega.1c03438

Notes

The authors declare no competing financial interest.

■ REFERENCES

(1) Wang, A.; Li, S.; Chen, H.; Hu, Y.; Peng, X. Synthesis and characterization of a novel microcrystalline cellulose-based polymeric bio-sorbent and its adsorption performance for Zn(II). *Cellulose* **2019**, *26*, 6849−6859.

(2) Guo, X.; Xu, D.; Yuan, H.-M.; Luo, Q.-Y.; Tang, S.-Y.; Liu, L.; Wu, Y.-Q. A novel fluorescent nanocellulosic hydrogel based on carbon dots for efficient adsorption and sensitive sensing in heavy metals. *J. Mater. Chem. A* **2019**, *7*, 27081−27088.

(3) Ibrahim, B. M.; Fakhre, N. A. Crown ether modification of starch for adsorption of heavy metals from synthetic wastewater. *Int. J. Biol. Macromol.* **2019**, *123*, 70−80.

(4) He, X.; Male, K. B.; Nesterenko, P. N.; Brabazon, D.; Paull, B.; Luong, J. H. T. Adsorption and Desorption of Methylene Blue on Porous Carbon Monoliths and Nanocrystalline Cellulose. *ACS Appl. Mater. Interfaces* **2013**, *5*, 8796−8804.

(5) Zhang, X.-F.; Elsayed, I.; Navarathna, C.; Schueneman, G.; Hassan, E.-B. Biohybrid Hydrogel and Aerogel from Self-Assembled Nanocellulose and Nanochitin as a High-Efficiency Adsorbent for Water Purification. *ACS Appl. Mater. Interfaces* **2019**, *11*, 46714−46725.

(6) Monier, M.; Ayad, D. M.; Sarhan, A. A. Adsorption of Cu(II), Hg(II), and Ni(II) ions by modified natural wool chelating fibers. *J. Hazard. Mater.* **2010**, *176*, 348−355.

(7) Hokkanen, S.; Bhatnagar, A.; Srivastava, V.; Suorsa, V.; Sillanpää, M. Removal of Cd^{2+}, Ni^{2+} and PO_4^{3-} from aqueous solution by hydroxyapatite-bentonite clay-nanocellulose composite. *Int. J. Biol. Macromol.* **2018**, *118*, 903−911.

(8) Deng, S.; Zhang, G.-S.; Wang, X.; Zheng, T.; Wang, P. Preparation and performance of polyacrylonitrile fiber functionalized with iminodiacetic acid under microwave irradiation for adsorption of Cu(II) and Hg(II). *Chem. Eng. J.* **2015**, *276*, 349−357.

(9) Wang, Y.; Wang, B.-X.; Wang, Q.-F.; Di, J.-C.; Miao, S.-D.; Yu, J.-H. Amino-Functionalized Porous Nanofibrous Membranes for Simultaneous Removal of Oil and Heavy-Metal Ions from Wastewater. *ACS Appl. Mater. Interfaces* **2019**, *11*, 1672−1679.

(10) Zietzschmann, F.; Stützer, C.; Jekel, M. Granular activated carbon adsorption of organic micro-pollutants in drinking water and treated wastewater e Aligning breakthrough curves and capacities. *Water Res.* **2016**, *92*, 180−187.

(11) Hu, X.-S.; Liang, R.; Sun, G.-X. Superadsorbent hydrogel for removal of methylene blue dye from aqueous solution. *J. Mater. Chem. A* **2018**, *6*, 17612−17624.

(12) Gu, H.-B.; Zhou, X.-M.; Lyu, S.-Y.; Pan, D.; Dong, M.-Y.; et al. Magnetic nanocellulose-magnetite aerogel for easy oil adsorption. *J. Colloid Interface Sci.* **2020**, *560*, 849−856.

(13) Muhammad, N.; Omar, W. N.; Man, Z.; Bustam, M. A.; Rafiq, S.; Uemura, Y. Effect of Ionic Liquid Treatment on Pyrolysis Products from Bamboo. *Ind. Eng. Chem. Res.* **2012**, *51*, 2280−2289.

(14) Shen, S.-C.; Nges, I. A.; Yun, J.-X.; Liu, J. Pre-treatments for enhanced biochemical methane potential of bamboo waste. *Chem. Eng. J.* **2014**, *240*, 253−259.

(15) Chen, S.; Zheng, Z.; Huang, P. Sustainable development for bamboo industry in Anji, Zhejiang Province of China. *Res. J. Environ. Sci.* **2011**, *5*, 279−287.

(16) Esfahani, M. R.; Taylor, A.; Serwinowski, N.; Parkerson, Z. J.; Confer, M. P.; Kammakakam, I.; Bara, J. E.; Esfahani, A. R.; Mahmoodi, S. N.; Koutahzadeh, N.; Hu, M.-Z. Sustainable Novel Bamboo-Based Membranes for Water Treatment Fabricated by Regeneration of Bamboo Waste Fibers. *ACS Sustainable Chem. Eng.* **2020**, *8*, 4225−4235.

(17) Hokkanen, S.; Bhatnagar, A.; Sillanpää, M. A review on modification methods to cellulose-based adsorbents to improve adsorption capacity. *Water Res.* **2016**, *91*, 156−173.

(18) Jiao, Y.; Wan, C.-C.; Li, J. Synthesis of carbon fiber aerogel from natural bamboo fiber and its application as a green high-efficiency and recyclable adsorbent. *Mater. Des.* **2016**, *107*, 26−32.

(19) Rajesh, Y.; Pujari, M.; Uppaluri, R. Equilibrium and Kinetic Studies of Ni(II) Adsorption using Pineapple and Bamboo Stem Based Adsorbents. *Sep. Sci. Technol.* **2014**, *49*, 533−544.

(20) Li, B.; Lv, J.-Q.; Guo, J.-Z.; Fu, S.-Y.; Guo, M.; Yang, P. The polyaminocarboxylated modified hydrochar for efficient capturing methylene blue and Cu(II) from water. *Bioresour. Technol.* **2019**, *275*, 360−367.

(21) Chen, Y.-F.; Ru, J.; Geng, B.-Y.; Wang, H.-Y.; Tong, C.-C.; Du, C.-G.; Wu, S.-C.; Liu, H.-Z. Charge-functionalized and mechanically durable composite cryogels from Q-NFC and CS for highly selective removal of anionic dyes. *Carbohydr. Polym.* **2017**, *174*, 841−848.

(22) Mahfoudhi, N.; Boufi, S. Nanocellulose as a novel nano-structured adsorbent for environmental remediation: a review. *Cellulose* **2017**, *24*, 1171−1197.

(23) Członkaa, S.; Bertino, M. F.; Kośny, J.; Strąkowska, A.; Masłowski, M.; Strzelec, K. Linseed oil as a natural modifier of rigid polyurethane foams. *Ind. Crops Prod.* **2018**, *115*, 40−51.

(24) Agrawal, A.; Kaur, R.; Walia, R. S. PU Foam Derived from Renewable Sources: Perspective on Properties Enhancement: An Overview. *Eur. Polym. J.* **2017**, *95*, 255−274.

(25) Hong, H.-J.; Lim, J. S.; Hwang, J. Y.; Kim, M.; Jeong, H. S.; Park, M. S. Carboxymethlyated cellulose nanofibrils (CMCNFs) embedded in polyurethane foam as a modular adsorbent of heavy metal ions. *Carbohydr. Polym.* **2018**, *195*, 136−142.

(26) Wu, L.-H.; Xie, Q.-Y.; Lv, Y.-B.; Zhang, Z.-Y.; Wu, Z.-Y.; Liang, X.-J.; Lu, M.-Z.; Nie, Y. Degradation of methylene blue by dielectric barrier discharge plasma coupled with activated carbon supported on polyurethane foam. *RSC Adv.* **2019**, *9*, 25967−25975.

(27) Ranote, S.; Kumar, D.; Nadda, S.; Kumar, R.; Chauhan, G. S.; Joshi, V. Green synthesis of Moringa oleifera gum-based bifunctional polyurethane foam braced with ash for rapid and efficient dye removal. *Chem. Eng. J.* **2019**, *361*, 1586−1596.

(28) Qiu, C.-P.; Li, F.; Wang, L.; Zhang, X.-L.; Zhang, Y.; Tang, Q.; Zhao, X.-Y.; De Hoop, C. F.; Peng, X.-P.; Yu, X.-J.; Huang, X.-Y. The preparation and properties of polyurethane foams reinforced with bamboo fiber sources in China. *Mater. Res. Express* **2021**, *8*, No. 045501.

(29) Wei, J.; Yang, Z.-X.; Sun, Y.; Wang, C.-K.; Fan, J.-L.; Kang, G.-Y.; Zhang, R.; Dong, X.-Y.; Li, Y.-F. Nanocellulose-based magnetic hybrid aerogel for adsorption of heavy metal ions from water. *J. Mater. Sci.* **2019**, *54*, 6709−6718.

(30) De Haro, J. C.; Chiara, A.; T Smit, A.; Turri, S.; D'Arrigo, P.; Griffini, G. Biobased Polyurethane Coatings with High Biomass Content: Tailored Properties by Lignin Selection. *ACS Sustainable Chem. Eng.* **2019**, *7*, 11700−11711.

(31) Huang, X.-Y.; De Hoop, C. F.; Xie, J.-L.; Wu, Q.-L.; Boldor, D.; Qi, J.-Q. High bio-content polyurethane (PU) foam made from bio-polyol and cellulose nanocrystals (CNCs) via microwave liquefaction. *Mater. Des.* **2018**, *138*, 11−20.

(32) Isachenko, A. I.; Apyar, V. V.; Melekhin, A. O.; Garshev, A. V.; Volkov, P. A.; Dmitrienko, S. G. Polyurethane foam modified with

borohydride: preparation and possibilities of using for synthesis of gold nanoparticles and their nanocomposites. *IOP Conf. Ser.: Mater. Sci. Eng.* **2019**, *704*, No. 012001.

(33) Xie, J.-L.; Hse, C. Y.; Li, C.-J.; Shupe, T. F.; Hu, T.-X.; Qi, J.-Q.; De Hoop, C. F. Characterization of Microwave Liquefied Bamboo Residue and Its Potential Use in the Generation of Nanofibrillated Cellulosic Fiber. *ACS Sustainable Chem. Eng.* **2016**, *4*, 3477−3485.

(34) Kairytė, A.; Kizinievič, O.; Kizinievič, V.; Kremensas, A. Synthesis of biomass-derived bottom waste ash based rigid biopolyurethane composite foams Rheological behaviour, structure and performance characteristics. *Composites, Part A* **2019**, *117*, 193−201.

(35) Zieleniewska, M.; Ryszkowska, J.; Bryśkiewicz, A.; Auguścik, M.; Szczepkowski, L.; Świderski, A.; Wrześniewska-Tosik, K. The structure and properties of viscoelastic polyurethane foams with Fyrol and keratin fibers. *Polimery* **2017**, *62*, 127−135.

(36) Kläusler, O.; Bergmeier, W.; Karbach, A.; Meckel, W.; Mayer, E.; Clauß, S.; Niemz, P. Influence of N,N-dimethylformamide on one-component moisture-curing polyurethane wood adhesives. *Int. J. Adhes. Adhes.* **2014**, *55*, 69−76.

(37) Li, B.; Zhou, M.-Y.; Huob, W.-Z.; Cai, D.; Qin, P.-Y.; Cao, H.; Tan, T.-W. Fractionation and oxypropylation of corn-stover lignin for the production of biobased rigid polyurethane foam. *Ind. Crops Prod.* **2020**, *143*, No. 111887.

(38) Mendoza, L.; Hossain, L.; Downey, E.; Scales, C.; Batchelor, W.; Garnier, G. Carboxylated Nanocellulose Foams as Superabsorbents. *J. Colloid Interface Sci.* **2019**, *538*, 433−439.

(39) Zhang, J.-M.; Hori, N.; Takemura, A. Optimization of agricultural wastes liquefaction process and preparing bio-based polyurethane foams by the obtained polyols. *Ind. Crops Prod.* **2019**, *138*, No. 111455.

(40) Mahmood, N.; Yuan, Z.-S.; Schmidt, J.; Charles Xu, C.-B. Preparation of bio-based rigid polyurethane foam using hydrolytically depolymerized Kraft lignin via direct replacement or oxypropylation. *Eur. Polym. J.* **2015**, *68*, 1−9.

(41) Huang, J.-K.; Young, W.-B. The mechanical, hygral, and interfacial strength of continuous bamboo fiber reinforced epoxy composites. *Composites, Part B* **2019**, *166*, 272−283.

(42) Sur, S. H.; Choi, P. J.; Ko, J. W.; Lee, J. Y.; Lee, Y. H.; Kim, H. D. Preparation and Properties of DMF-Based Polyurethanes for Wet-Type Polyurethane Artificial Leather. *Int. J. Polym. Sci.* **2018**, *2018*, 1−9.

(43) Fallah, Z.; Isfahani, H. N.; Tajbakhsh, M.; Tashakkorian, H.; Amouei, A. TiO$_2$-grafted cellulose via click reaction: an efficient heavy metal ions bioadsorbent from aqueous solutions. *Cellulose* **2018**, *25*, 639−650.

(44) Tian, H.-Y.; Liu, Z.-G.; Zhang, M.; Guo, Y.-L.; Zheng, L.; Li, Y.-C.-C. Biobased Polyurethane, Epoxy Resin, and Polyolefin Wax Composite Coating for Controlled-Release Fertilizer. *ACS Appl. Mater. Interfaces* **2019**, *11*, 5380−5392.

(45) Zhang, C.-Q.; Kessler, M. R. Bio-based Polyurethane Foam Made from Compatible Blends of Vegetable-Oil-based Polyol and Petroleum-based Polyol. *ACS Sustainable Chem. Eng.* **2015**, *3*, 743−749.

(46) Guo, A.; Javni, I.; Petrovic, Z. Rigid Polyurethane Foams Based on Soybean Oil. *J. Appl. Polym. Sci.* **2000**, *77*, 467−473.

(47) Yang, H.-P.; Yan, R.; Chen, H.-P.; Lee, D. H.; Zheng, C.-G. Characteristics of hemicellulose, cellulose and lignin pyrolysis. *Fuel* **2007**, *86*, 1781−1788.

(48) Kumari, S.; Chauhan, G. S.; Ahn, J. H. Novel cellulose nanowhiskers-based polyurethane foam for rapid and persistent removal of methylene blue from aqueous solutions. *Chem. Eng. J.* **2016**, *304*, 728−736.

(49) Huang, X.-Y.; De Hoop, C. F.; Xie, J.-L.; Hse, C. Y.; Qi, J.-Q.; Chen, Y.-Z.; Li, F. Thermal decomposition characteristics of microwave liquefied rape straw residues using thermogravimetric analysis. *J. Therm. Anal. Calorim.* **2018**, *131*, 1911−1918.

(50) Wang, S.-K.; Ma, X.-F.; Zheng, P.-W. Sulfo-functional 3D porous cellulose/graphene oxide composites for highly efficient

removal of methylene blue and tetracycline from water. *Int. J. Biol. Macromol.* **2019**, *140*, 119−128.

(51) Yang, X.; Liu, H.; Han, F.-Y.; Jiang, S.; Liu, L.-F.; Xia, Z.-P. Fabrication of cellulose nanocrystal from Carex meyeriana Kunth and its application in the adsorption of methylene blue. *Carbohydr. Polym.* **2017**, *175*, 464−472.

(52) Huang, X.-Y.; De Hoop, C. F.; Xie, J.-L.; Hse, C. Y.; Qi, J.-Q.; Hu, T.-X. Characterization of Biobased Polyurethane Foams Employing Lignin Fractionated from Microwave Liquefied Switchgrass. *Int. J. Polym. Sci.* **2017**, *2017*, No. 4207367.

(53) Bernal, V.; Giraldo, L.; Moreno-Piraján, J. C. Physicochemical Parameters of the Methylparaben Adsorption from Aqueous Solution Onto Activated Carbon and Their Relationship with the Surface Chemistry. *ACS Omega* **2021**, *6*, 8797−8807.

(54) Saha, T. K.; Bishwas, R. K.; Karmaker, S.; Islam, Z. Adsorption Characteristics of Allura Red AC onto Sawdust and Hexadecylpyridinium Bromide-Treated Sawdust in Aqueous Solution. *ACS Omega* **2020**, *5*, 13358−13374.

(55) Huang, X.-Y.; De Hoop, C. F.; Li, F.; Xie, J.-L.; Hse, C. Y.; Qi, J.-Q.; Jiang, Y.-Z.; Chen, Y.-Z. Dilute Alkali and Hydrogen Peroxide Treatment of Microwave Liquefied Rape Straw Residue for the Extraction of Cellulose Nanocrystals. *J. Nanomater.* **2017**, *2017*, 1−9.

(56) Mo, L.-T.; Pang, H.-W.; Tan, Y.; Zhang, S.-F.; Li, J.-Z. 3D multi-wall perforated nanocellulose-based polyethylenimine aerogels for ultrahigh efficient and reversible removal of Cu(II) ions from water. *Chem. Eng. J.* **2019**, *378*, No. 122157.

(57) Zhao, F.-P.; Repo, E.; Song, Y.; Yin, D.-L.; Hammouda, S. B.; Chen, L.; Kalliola, S.; Tang, J.-T.; Tam, K. C.; Sillanpää, M. Polyethylenimine-cross-linked cellulose nanocrystals for highly efficient recovery of rare earth elements from water and mechanism study. *Green. Chem.* **2017**, *19*, 4816−4828.

(58) Burks, T.; Avila, M.; Akhtar, F.; Göthelid, M.; Lansåker, P. C.; Toprak, M. S.; Muhammed, M.; Uheida, A. Studies on the adsorption of chromium(VI) onto 3-Mercaptopropionic acid coated superparamagnetic iron oxide nanoparticles. *J. Colloid Interface Sci.* **2014**, *425*, 36−43.

(59) Safavi-Mirmahalleh, S. A.; Salami-Kalajahi, M.; Roghani-Mamaqani, H. Effect of surface chemistry and content of nanocrystalline cellulose on removal of methylene blue from wastewater by poly(acrylic acid)/nanocrystalline cellulose nanocomposite hydrogels. *Cellulose* **2019**, *26*, 5603−5619.

(60) Zhou, G.-Y.; Luo, J.-M.; Liu, C.-B.; Chu, L.; Ma, J.-H.; Tang, Y.-H.; Zeng, Z.-B.; Luo, S.-L. A highly efficient polyampholyte hydrogel sorbent based fixed-bed process for heavy metal removal in actual industrial effluent. *Water Res.* **2016**, *89*, 151−160.

(61) Pan, L.-T.; Zhai, G.-Z.; Yang, X.-R.; Yu, H.-R.; Cheng, C.-J. Thermosensitive Microgels-Decorated Magnetic Graphene Oxides for Specific Recognition and Adsorption of Pb(II) from Aqueous Solution. *ACS Omega* **2019**, *4*, 3933−3945.

(62) Zhang, N.; Zang, G.-L.; Shi, C.; Yu, H.-Q.; Sheng, G.-P. A novel adsorbent TEMPO-mediated oxidized cellulose nanofibrils modified with PEI: Preparation, characterization, and application for Cu(II) removal. *J. Hazard. Mater.* **2016**, *316*, 11−18.

(63) D'Halluin, M.; Rull-Barrull, J.; Bretel, G.; Labrugere, C.; Grognec, E. L.; Felpin, F. X. Chemically Modified Cellulose Filter Paper for Heavy Metal Remediation in Water. *ACS Sustainable Chem. Eng.* **2017**, *5*, 1965−1973.

(64) Hu, T.; Liu, Q.-Z.; Gao, T.-T.; Dong, K.-J.; Wei, G.; Yao, J.-S. Facile Preparation of Tannic Acid−Poly(vinyl alcohol)/Sodium Alginate Hydrogel Beads for Methylene Blue Removal from Simulated Solution. *ACS Omega* **2018**, *3*, 7523−7531.

(65) Setyono, D.; Valiyaveettil, S. Functionalized Paper-A Readily Accessible Adsorbent for Removal of Dissolved Heavy Metal Salts and Nanoparticles from Water. *J. Hazard. Mater.* **2016**, *302*, 120−128.

(66) Zhu, L.; Zhu, P.-H.; You, L.-J.; Li, S.-J. Bamboo shoot skin: turning waste to a valuable adsorbent for the removal of cationic dye from aqueous solution. *Clean Technol. Environ. Policy* **2019**, *21*, 81−92.

(67) Saha, P. Assessment on the Removal of Methylene Blue Dye using Tamarind Fruit Shell as Biosorbent. *Water, Air, Soil Pollut.* **2010**, *213*, 287−299.

(68) Pehlivan, E.; Altun, T.; Parlayici, S. Modified barley straw as a potential biosorbent for removal of copper ions from aqueous solution. *Food Chem.* **2012**, *135*, 2229−2234.

(69) Ben-Ali, S.; Jaouali, I.; Souissi-Najar, S.; Ouederni, A. Characterization and adsorption capacity of raw pomegranate peel biosorbent for copper removal. *J. Cleaner Prod.* **2017**, *142*, 3809−3821.

(70) Dai, C.-G.; Zhang, M.-H.; Guo, X.-W.; Ma, X.-X. Mesoporous composite Ni-C-N/SA for selective adsorption of methylene blue from water. *Chem. Eng. J.* **2021**, *407*, No. 127181.

(71) Jawad, A. H.; Abdulhameed, A. S. Mesoporous Iraqi red kaolin clay as an efficient adsorbent for methylene blue dye: Adsorption kinetic, isotherm and mechanism study. *Surf. Interfaces* **2020**, *18*, No. 100422.

(72) Jiang, L.; Wen, Y.-Y.; Zhu, Z.-J.; Liu, X.-F.; Shao, W. A Double cross-linked strategy to construct graphene aerogels with highly efficient methylene blue adsorption performance. *Chemosphere* **2021**, *265*, No. 129169.

(73) Chen, X.; Huang, Z.; Luo, S.-Y.; Zong, M.-H.; Lou, W.-Y. Multi-functional magnetic hydrogels based on Millettia speciosa Champ residue cellulose and Chitosan: Highly efficient and reusable adsorbent for Congo red and Cu^{2+} removal. *Chem. Eng. J.* **2021**, *423*, No. 130198.